Axisymmetric modes, fast ions and X-point effects in tokamak plasmas

Axisymmetric modes, fast ions and X-point effects in tokamak plasmas

Journal of Physics: Conference Series **2397** (2022) 012021 doi:10.1088/1742-6596/2397/1/012021

Axisymmetric modes, fast ions and X-point effects in tokamak plasmas

T. Barberis[1], F. Porcelli[1], R. Fitzpatrick[2], A. Yolbarsop[3]

[1] DISAT, Polytechnic University of Turin, Torino 10129, Italy
[2] IFS, University of Texas at Austin, USA
[3] KTX and USTC, Hefei, Anhui 230022, People's Republic of China

E-mail: `francesco.porcelli@polito.it`

Abstract.

Recent progress on the understanding of axisymmetric pertubations in tokamak plasmas is presented, with particular attention on Vertical Displacement Oscillatory Modes (VDOM) that can be driven unstable by their resonance with fast ion orbits, and on the impact of divertor X-points on the stability of vertical displacements.

1. Introduction

Renewed interest in axisymmetric modes has been prompted by the observation of saturated fluctuations with toroidal mode number $n = 0$ in ICRH and NBI heated JET plasmas, where MeV ions are produced [1, 2]. Furthermore, an interesting and until now little studied problem concerns the singular behavior of divertor X-points to $n = 0$ perturbations, which is likely to give rise to axisymmetric current sheets localized in the vicinity of the divertor X-points and along the magnetic separatrix [3]. This article focuses on recent progress in the understanding of these two aspects.

Recent progress on the development of analytic theory for $n = 0$ modes is reviewed. Particular attention is given to the resonant excitation of VDOM by energetic ions, which requires a fast ion distribution with a positive slope as a function of energy. As also pointed out by other authors [2, 4], a positive slope can be produced when the fast ion source is modulated on time scales that are short compared with the fast ion slowing down time. Here, we show that source modulation by sawtooth oscillations can lead to the same result. In the final part of this article, we discuss the effect of the ideal-MHD X-point resonance on $n = 0$ modes.

This article is organized as follows. The equilibrium scenarios and model equations are discussed in Sec. 2. A general dispersion relation that includes the effects of a nearby resistive wall is derived in Sec. 3. Fast ion effects are discussed in Sec. 4. In Sec. 5, we focus on mechanisms leading to the formation of fast ion distributions with a positive slope as a function of energy. X-point effects are discussed in Sec. 6. Conclusions are presented in Sec. 7.

2. Equilibrium: limiter and divertor scenarios

Analytic theory is possible if a relatively simple equilibrium configuration is adopted. With reference to Fig. 1, we assume the plasma current density to be uniform up to a *convenient* elliptical flux surface, and zero outside. The analytic solution for the equilibrium flux function

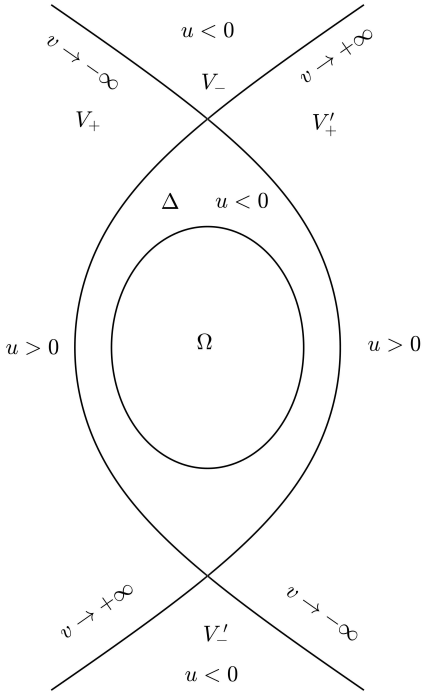

Figure 1. Equilibrium configuration

in elliptical coordinates (μ, θ) was derived in Ref [5]. We distinguish two scenarios of interest. In the first scenario, which we call the *limiter* scenario, the plasma density is also assumed to be constant and to drop to zero at the convenient elliptical surface, which is then the actual plasma boundary with $\mu = \mu_b$. The region Ω, displayed in Fig. 1, describes the whole volume occupied by the plasma including its boundary, i.e. up to $\mu_b + \epsilon$. A nearby wall, not shown in the figure, modeled as a confocal ellipse surrounds the plasma. The stability of this configuration on the basis of the ideal MHD energy principle for an ideal wall was studied by Laval et al in classic paper [6]. Recently [7], we have extended the work of Ref. [6] by assuming a resistive wall and normal mode analysis, which leads to a cubic dispersion relation for the mode frequency (see Sec. 3). In the second scenario [3, 8], the *divertor* scenario, the uniform plasma density extends to the magnetic separatrix, which therefore is the actual plasma boundary. In this case, perturbed currents can be driven along the separatrix and X-point effects become important. This scenario is briefly discussed in Sec. 6.

Normal mode analysis is carried out on the basis of the standard reduced ideal MHD model [9]. Fast ion effects are introduced perturbatively according to kinetic-MHD as described in Sec. 4.

3. Dispersion relation in the limiter scenario

In this section, with the help of quadratic forms, we derive a dispersion relation for $n = 0$ vertical modes in the *limiter* scenario for arbitrary values of the ellipticity parameter

$$e_0 = \frac{b^2 - a^2}{b^2 + a^2}, \tag{1}$$

with plasma elliptical boundary minor and major semi-axes a and b. The dispersion relation depends on geometrical parameters and on a function, $D_w(\gamma)$, determined by the geometry and the resistivity of the wall, which becomes independent of γ in the ideal wall limit.

$$-\gamma^2 = \frac{\delta W_{core}(\gamma) + \delta W_{fast}(\gamma)}{\delta I}, \tag{2}$$

where δI is defined as $\int_\Omega \rho_m \xi^2/2$, with mass density ρ_m and plasma displacement ξ. The $\delta W_{core}(\gamma)$ includes the wall effects and becomes dependent on γ when the wall resistivity is taken into account. The fast ion contribution, δW_{fast}, is neglected in this section.

The core contribution to δW following the *limiter* scenario equilibrium described in [7] can be written as:

$$\delta W = \frac{1}{2}\int_\Omega d^3x \left(\mathbf{e}_z \times \frac{\nabla\tilde{\varphi}^*}{\gamma^*}\right) \cdot (\tilde{J}\nabla\psi_{eq} + J_{eq}\nabla\tilde{\psi}), \tag{3}$$

where $\tilde{\varphi}^*$ is the complex conjugate of the perturbed stream function and $\tilde{\psi}$ is the perturbed magnetic flux. The stabilizing effects of the passive wall are included in the total plasma displacement of which both perturbed quantities depend. The eddy currents induced in the wall generate a contribution to the perturbed flux, which in turn is consistent with part of the plasma displacement, denoted by ξ_{ext}, that opposes the vertical plasma displacement. As shown in [7], the total plasma displacement is the combination of the *no-wall* displacement and this external contribution: $\xi = \xi_\infty - \xi_{ext}$.

From Eq. 3 one can thus obtain:

$$\delta W_{core} = -\frac{\pi}{2} L_z \frac{1 - a/b}{ab} \frac{1 - D_w(\gamma)}{1 - \hat{e}_0 D_w(\gamma)} \xi^2, \tag{4}$$

where $\hat{e}_0 = e_0 b/(a+b)$. The parameter $D_w(\gamma)$ takes into account the resistive wall effects and it is defined as:

$$D_w = \frac{\xi_{ext}}{\hat{e}_0 \xi_\infty} = D\frac{\gamma\tau_\eta}{1 + \gamma\tau_\eta}. \tag{5}$$

If the wall providing passive feedback stabilization is ideal (resistive wall time $\tau_\eta \to \infty$), $D_w(\gamma)$ reduces to a geometrical factor D, that depends on wall position and geometry. In the *no-wall* limit in which the wall distance becomes very large, the external contribution to the plasma displacement ξ_{ext} vanishes and $D \to 0$. The maximum value for the parameter D is obtained when the wall coincides exactly with the plasma boundary. In this limit, $D = D_{max} = 1/\hat{e}_0$ and the denominator in Eq. (4) vanishes together with the amplitude of the displacement, $\xi = \xi_\infty - \xi_{ext}$, as $\xi_{ext} \to \xi_\infty$. For an elongation $b/a = 1.4$, this maximum value is $D_{max} \approx 5.3$. For an elliptical wall confocal to the plasma boundary with $a_w/a \approx 1.3$, then $D \approx 3.5$.

Using Eq. 4, the dispersion relation for axisymmetric modes in the *limiter* scenario can be written in dimensional form as:

$$(\gamma\tau_A)^2 = \frac{r_0^4}{a^2 b^2}\left(1 - \frac{a}{b}\right)\frac{1 - D_w}{1 - \hat{e}_0 D_w}, \tag{6}$$

where $r_0 = a\,b/[\left(a^2 + b^2\right)/2]^{1/2}$ and τ_A is the poloidal Alfvén time. This dispersion relation is "general", in the sense that it can be applied to the three cases of interest, i.e., the no-wall limit, the ideal wall case, and the resistive wall case, as wall effects are included through the single stability parameter, D_w.

In the relevant case of nearby resistive wall, the dispersion relation of Eq. 6 becomes a cubic. The stabilization of the ideal vertical instability requires the geometrical parameter $D > 1$. Thus, the solutions of the dispersion relation correspond to a purely growing mode on resistive wall time scales $\gamma = 1/(D-1)\tau_\eta$, which is typically suppressed by means of active feedback stabilization, and two oscillatory roots described by:

$$\omega = \pm\omega_0 - i\frac{1}{2\tau_\eta}\frac{D(1-\hat{e}_0)}{(D-1)(1-\hat{e}_0 D)}. \tag{7}$$

These two roots corresponds to oscillatory modes in the vertical direction damped on resistive wall timescales that we will refer as Vertical Displacemens Oscillatory Mode (VDOM). Their oscillation frequency ω_0 is Alfvénic, and defined as:

$$\omega_0 = \left[\frac{D-1}{1-\hat{e}_0 D}(1-e_0)(1+e_0-\sqrt{1-e_0^2}\,)\right]^{1/2}\tau_A^{-1} \tag{8}$$

For typical JET parameters this frequency is of the order of hundreds of kHz.

4. Fast-ion resonance

In this section we focus our attention on the oscillatory solutions of the dispersion relation. In the situation in which the ideal vertical instability is stabilized by a nearby wall, vertical displacement oscillatory modes (VDOM) are damped by wall resistivity. Their oscillation frequency is slightly below the poloidal Alfvén frequency, and as such they are not affected by continuum damping. This opens the possibility of a resonant interaction with MeV fast ions leading to a destabilization of these modes, as discussed in [10]. The derivation of the dispersion relation in terms of quadratic forms presented in the previous section allows for a straightforward introduction of fast-ion resonant effects via a perturbative approach within the hybrid kinetic-MHD model, where fast ions are described according to drift kinetics. Therefore, in Eq. 2 we consider only the immaginary contribution to the mode growth rate coming from the fast ions term δW_{fast}. The dispersion relation for the oscillatory VDOM is then modified by the wave-particle resonance, and reads:

$$\omega^2 = \omega_0^2 - 2i\omega_0\gamma_\eta + i\omega_0^2\lambda_h + \mathcal{O}(\gamma^2/\omega_0^2), \tag{9}$$

where γ_η is the inverse resistive wall time. The dimensionless parameter $\lambda_h = \mathcal{I}m(\delta W_h) \ll 1$ depends only on the so called *non-adiabatic* part of δW_{fast}, which describes the resonance, defined in Eq. 10:

$$\delta W_h = \zeta \sum_\sigma \int dP_\phi d\mathcal{E} d\mu_\perp \tau_\Omega \omega \frac{\partial F}{\partial \mathcal{E}} \sum_{p=-\infty}^{+\infty} \frac{|\Upsilon_p|^2}{\omega + p\omega_\Omega}. \tag{10}$$

Here ζ is a normalization constant, the summation is over co- and counter particles and the integration is performed over the three invariants of the fast ion motion, i.e. canonical toroidal momentum P_ϕ, energy $\mathcal{E}$ and magnetic moment $\mu_\perp$. The sum over p comes from the fourier expansion of the fast particle lagrangian over their orbit periodicity, Υ_p are the Fourier coefficients and the denominator shows clearly the resonance condition between the mode frequency ω and the passing/trapped orbit frequency $\omega_\Omega = 2\pi\tau_\Omega^{-1}$. Due to the fact that we are considering $n = 0$ modes, the sign of δW_h, and thus of λ_h, depends only on the derivative of the fast ion distribution function with respect to the energy, $\partial F/\partial\mathcal{E}$. As shown in details in Ref. [10], the destabilization

of the VDOM due to wave-particle resonance requires $\partial F/\partial \mathcal{E} > 0$. In the next section we focus our attention on how to obtain a fast ion distribution function with this characteristic.

5. $\partial F/\partial E > 0$: Losses and source modulation

A fast ion distribution function with positive slope, like the one required for the destabilization of the VDOM, is not the standard slowing distributions function (the standard slowing down distribution would result in VDOM damping). In this section we focus on two mechanisms that lead to a fast ion distribution function with positive slope with respect to the energy: fast ion *losses* and *source modulation*. The first mechanism is the one discussed in Ref. [10]. If the fast ions are lost fast enough with respect to their slowing down time τ_{sd}, the usual slowing down distribution function cannot form, and a situation with $\partial F/\partial \mathcal{E} > 0$ can be achieved. Considering a constant loss term ν_{loss}, it is possible to show that the distribution function as a function of the velocity for a monochromatic source term at $v = v_{fast}$, reads:

$$F(v) \propto H(v_{fast} - v)/(v^3 + v_c^3)^{1-\alpha}, \tag{11}$$

where v_c is the critical velocity and $\alpha = \tau_{sd}\nu_{loss}/3$. Thus, when $\alpha > 1$, the resonant interaction with fast ions can lead to the excitation of fast ion driven vertical modes (in brief, FIDVM).

The second mechanism consists in the modulation of the source of fast ions on a time scale shorter than τ_{sd}. This can be done, for instance, considering the modulation of heating systems, as discussed in [4]. In the case of fusion-born alphas, a natural modulation is associated with sawtooth oscillations [2]. In the following, we focus on this second mechanism. The time evolution of the q and thermal pressure profiles is modeled analytically according to Kadomtsev's sawtooth model [11]. Assuming parabolic q and p profiles evolving along the sawtooth ramp, the reconnected profiles after the sawtooth crash can be determined analitically, as showed for the pressure profile in Fig. 2. The thermal plasma pressure is redistributed within the sawtooth mixing radius. Assuming triangular sawtooth traces as funtion of time, the pressure profile recovers linearly in time along the ramp. On the other hand, in the limit where the fast ion precession frequncy is large as compared to the sawtooth crash time, high energy alpha particles are not affected Kadomtsev radial mixing and remain confined in the core, as discussed in [12].

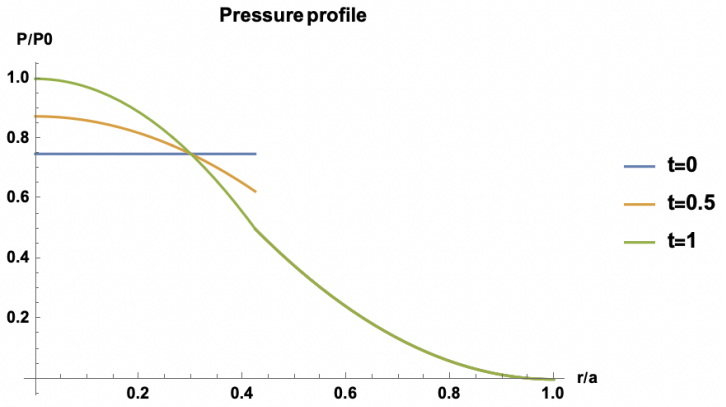

Figure 2. Pressure evolution during a sawtooth cycle

In the Fokker-Plank equation, the source term for fusion alpha particles is proportional to the square of the thermal plasma pressure. Therefore, the alpha distribution function becomes periodic in time, with period equal to the sawtooth period, τ_{saw}. After standard manipulations,

the equation for the tail ($v > v_c$) of the alpha distribution function $f(r, v, t)$ reads:

$$\frac{\partial v^3 f}{\partial t} - \frac{v}{\tau_s}\frac{\partial v^3 f}{\partial v} + \nu_\alpha v^3 f = v^3 S(r, v, t) \tag{12}$$

Figure 3 shows the solution of Eq. 12 as a function of velocity for a fixed time, with and without the effect of the source modulation.

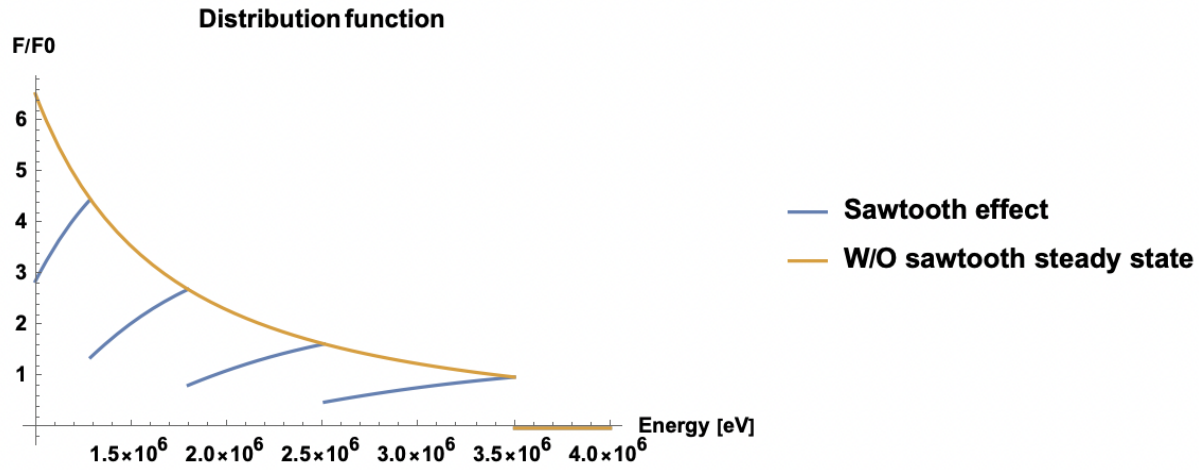

Figure 3. Normalized distribution function as a function of energy considering a loss term $\alpha = 0.5$ and $\tau_{saw}/\tau_{sd} = 1/3$

On a timescale shorter than τ_{sd}, this effect, together with a loss rate $\alpha = 0.5$, leads to a time dependent distribution function with regions of positive slope with respect to the energy. This mechanism is capable of providing an instability drive for the $n = 0$ modes observed in JET experiments [**?**]. Indeed, in these sawtoothing experiments, the sawtooth period was $\tau_{saw} \sim 100ms$, while the slowing down time of $\tau_{sd} \sim 300ms$.

6. The divertor scenario: X-point effects

The impact of divertor X-points on the stability of vertical displacements was studied in detail in Refs. [3, 8]. The algebra is rather complex. Here, we summarize the main results.

With reference to Fig. 1, in region Δ and in the vacuum regions V, it is convenient to introduce flux coordinates:

$$u = \alpha^{-2}[\psi^+_{eq}(\mu, \theta) - \psi_X], \tag{13}$$

$$v = \theta - \frac{\pi}{2} + \frac{e_0}{2}\cosh[\,2(\mu - \mu_b)\,]\sin(2\theta), \tag{14}$$

where ψ^+_{eq} is the equilibrium magnetic flux beyond region Ω, $\psi^+_{eq} = \psi_X$ corresponds to the magnetic separatrix, and $\mu = \mu_b$ is the *convenient* elliptical surface. Magnetic X-points have coordinates $u = 0$, $v = 0, \pi$. We concentrate on local behavior near the upper X-point at $v = 0$. Normal mode analysis, detailed in Refs. [3, 8], reveals the development of a current sheet along the magnetic separatrix:

$$j_X(v) \sim -\frac{2e_0}{ab}\sqrt{\frac{\pi}{2}}\left(\frac{p}{2} + q\right)\frac{\xi}{b}\,|v|^{1/2}\delta(u) \quad \text{as} \quad v \to 0, \tag{15}$$

where ξ is the plasma displacement and

$$p = [(a^2 + b^2)/\pi a^2]^{1/2}(1 - e_0^2)^{-1/4} e_0^{1/2} \tag{16}$$

is a positive parameter that scales as $e_0^{1/2}$. The second parameter q can be determined considering the parity of the perturbed flux along the magnetic separatrix as function of v: $q = \pm p/2$ for even and odd parity respectively. The dispersion relation is

$$\gamma^2 = -2\sqrt{\frac{\pi a}{2b}} \left(q + \frac{p}{2}\right) \left(1 - e_0^2\right)^{1/2} e_0^{3/2} \omega_A^2 \tag{17}$$

We find two classes of modes, depending on the parity of the perturbed flux:

- odd solutions, $q = -p/2$, the current sheet is absent and the growth rate vanishes, $\gamma^2 = 0$;
- even solution, $q = p/2$, a current sheet is present and $\gamma^2 < 0$, only two oscillatory solutions are found.

For the latter case, the current sheet that develops near the X-point and along the magnetic separatrix is capable of providing passive feedback stabilization even in the absence of a nearby wall! Noting that current sheets always form at the plasma boundary, it was argued in Ref. [8] that the nature of the current sheet changes as the plasma boundary approaches the magnetic separatrix. A magnetic flux surface $u = u_{marg}$, with u_{marg} small ($u = 0$ corresponding to the separatrix), must exist, such that, when the plasma boundary is at $u = u_{marg}$, marginal ideal-MHD stability against vertical perturbations is obtained for the no-wall case. The relevant analysis is carried out in Ref [8].

Current sheets have been observed in numerical simulations of the vertical instability in tokamaks, with advanced numerical codes that treat correctly the X-point geometry such as M3D-C[1], NIMROD and JOREK (see, e.g., [13]). However, analytic understanding of why these current sheets form, and the impact they have on the stability of vertical displacements, was not clarified in those numerical works.

7. Conclusions

In this article, recent progress on the analytic understanding of $n = 0$ modes in tokamak plasma has been discussed. The article reports five main results.

(1) A general dispersion relation for vertical displacement normal modes has been derived analytically. Vertical displacements cause an up-down motion of the entire plasma column, and as such are dominated by Fourier components with elliptical mode number $m = 1$. The method of quadratic forms, together with the normal-mode solution for the mode structure, are shown to be an expedient way to obtain the relevant dispersion relation. The latter contains a parameter, $D_w(\gamma)$, which is a function of the complex mode eigenvalue, $\gamma = -i\omega$, for the case of plasma confined by a resistive wall, see Eq. (5). D_w reduces to a constant D parameter in the limit of an ideal wall, see Eq. (5). When the wall is moved to infinity (the no-wall case), $D \to 0$. It follows that the relevant dispersion relation is quadratic in γ for the case of an ideal wall (including the no-wall limit), while it is cubic in γ for the case of a resistive wall. Thus, an additional root (compared to the ideal wall limit) is found for the resistive wall case. This root corresponds to a zero frequency, purely growing mode, with a growth time of the order of the resistive wall time. Active feedback control systems applied to vertical modes in tokamak experiments concentrate on the suppression of this purely growing mode [14].

(2) The other two roots, that we have dubbed "vertical displacement oscillatory modes", or VDOM, are purely oscillatory for the case of an ideal wall, provided the parameter D is larger than unity, which sets a condition on the distance of the ideal wall from the plasma. The

oscillation frequency is slightly below the poloidal Alfvén frequency, which makes these modes immune to Alfvén continuum damping and only weakly damped by wall resistivity.

(3) On the other hand, VDOM can interact resonantly with fast ion populations, which are present in a tokamak plasma due to auxiliary heating and/or as fusion reaction products. Under special circumstances, this resonant interaction gives rise to a new fast ion instability, dubbed fast-ion-driven vertical mode, or FIDVM. Indeed, the theory presented in this article is motivated in part by the observation of saturated $n = 0$ fluctuations, with a frequency of the order of the poloidal Alfvén frequency, in recent JET experiments where fast ions are produced by auxiliary heating, see Refs. [1, 2]. In those articles, the observations were tentatively interpreted in terms of a saturated $n = 0$ Global Alfvén Eigenmode (GAE) [15]. It is early for us to conclude whether, in fact, the mode observed at JET is a VDOM driven unstable by the fast ion resonance, rather than a GAE. More experiments are required, but also, the theory presented here ought to be developed further. Nevertheless, we can indicate the main points of distinction between GAE and VDOM that may facilitate the experimental identification. These are basically three. First, the GAE mode frequency for $n = 0$ is given by [15] $\omega_{GAE} = v_A/qR = \tau_A^{-1}$, where τ_A is the poloidal Alfvén time. On the other hand, the VDOM mode frequency is given by Eq. (7), and, taking the parameter D above unity, but anyway of order unity, it falls below the GAE mode frequency, since the ellipticity parameter e_0 is typically small. Secondly, the VDOM frequency scales as the square root of e_0, while the $n = 0$ GAE mode frequency is independent of elongation. Indeed, the GAE would survive in the circular limit, while the VDOM would not. Thirdly, and perhaps most importantly, the VDOM mode structure is different from that of the GAE. The VDOM is a vertical mode, corresponding to a vertical oscillation of the plasma cross-section, with the relevant perturbed flux an odd function of the poloidal angle. This signature would be easily detected by magnetic perturbation coils placed on top and bottom of the plasma column. The GAE mode structure favors instead a ballooning type of parity, with the perturbed flux being an even function of the poloidal angle.

(4) The FIDVM are excited when the fast ion distribution function develops a positive slope as a function of energy. This may occur in three situations of interest: (i) sources of auxiliary NBI and/or ICRH, which produce fast ion populations in current experiments, are modulated on time scales that are short compared with the fast ion slowing down time, τ_{sd}; (ii) a natural modulation occurs due to sawtooth activity, in the regime where $\tau_{saw} < \tau_{sd}$. This may be particularly relevant at JET, as well as for ITER and other future fusion experiments; (iii) Fast particles are not well confined and are lost before they have completely slowed-down. The most relevant scenario is probably a combination of the three situations described above.

(5) Finally, for the case where a magnetic divertor separatrix limits the plasma, it was found in Ref. [3, 8] that, even for the no-wall case, axisymmetric current sheets localized in the vicinity of the magnetic X-point(s) on the divertor separatrix, induced by vertical displacement perturbations, lead to passive feedback stabilization of vertical modes. The reason is that X-points are resonant points for ideal-MHD perturbations with toroidal mode number $n = 0$. As a result, flux pile-up will occur in the presence of ideal-MHD flows having the vertical symmetry around the resonant points. Flux pile-up is the reason for the occurrence of current sheets, which have the appropriate sign and magnitude to "push back" the plasma drifting vertically towards a magnetic X-point. In this sense, these X-point currents have the same effect on the plasma as that of image currents induced by vertical displacements on an ideal (or nearly ideal) wall.

Acknowledgements.

This work has been carried out within the framework of the EUROfusion Consortium and has received funding from the Euratom Research and Training Programme (Grant Agreement No 101052200 — EUROfusion). Views and opinions expressed are however those of the authors only and do not necessarily reflect those of the European Union or the European Commission. Neither the European Union nor the European Commission can be held responsible for them.

This work was partially supported by the National Natural Science Foundation of China under Grant No.11775220 and the National Magnetic Confinement Fusion Energy Development Program of China under Grant No.2017YFE0301702.

References

[1] Oliver H J C, Sharapov S E, Breizman B N and Zheng L J 2017 *Physics of Plasmas* **24** 122505
[2] Kiptily V G e a 2021 *Nucl. Fusion* **61** 114006
[3] Yolbarsop A, Porcelli F and Fitzpatrick R 2021 *Nucl. Fusion* **61** 114003
[4] Van Zeeland M A, Bardoczi L, Gonzalez-Martin J, Heidbrink W, Podesta M, Austin M, Collins C, Du X, Duarte V, Garcia-Munoz M, Munaretto S, Thome K, Todo Y and Wang X 2021 *Nucl. Fusion* **61** 066028
[5] Porcelli F and Yolbarsop A 2019 *Phys. Plasmas* **26** 054501
[6] Laval G, Pellat R and Soule J L 1974 *Phys. Fluids* **17** 835
[7] Barberis T, Porcelli F and Yolbarsop A 2022 *Accepted for publication in J. Plasma Phys.*
[8] Yolbarsop A, Porcelli F, Liu W and Fitzpatrick R 2022 *Plasma Phys. Contr. Fusion* **64** 105002
[9] Strauss H R 1976 *Phys. Fluids* **19** 134
[10] Barberis T, Porcelli F and Yolbarsop A 2022 *Nucl. Fusion* **62** 064002
[11] Kadomtsev B B 1975 *Fiz. Plazmy* **1** 710 [Sov. J. Plasma. Phys. **1** 389 (1975)]
[12] Bierwage A, Shinohara K, Kazakov Y and *et al* 2022 *Nat Commun* **13** 3941
[13] Krebs I e al 2020 *Phys. Plasmas* **10** 930
[14] Albanese R Mattei M and Villone F 2004 *Nucl. Fusion* **44** 999
[15] Villard L and Vaclavik J 1997 *Nucl. Fusion* **37**(3)